PNAS
www.pnas.org

Supplementary Information for

Human Embryonic Stem Cell-Derived Organoid Retinoblastoma Reveals a Cancerous Origin

Hui Liu, Yan Zhang, You-You Zhang, Yan-Ping Li, Zi-Qi Hua, Chang-Jun Zhang, Kun-Chao Wu, Fulong Yu, Yaru Zhang, Jianzhong Su, and Zi-Bing Jin

Corresponding Author: Zi-Bing Jin. E-mail: jinzibing@foxmail.com or Jianzhong Su. E-mail: sujz@wmu.edu.cn.

This PDF file includes:

Supplementary text

Figures S1 to S8

Legends for Figures S1 to S8

Tables S1 to S2

Legends for Tables S1 to S2

Legends for Movies S1 to S3

Other supplementary materials for this manuscript include the following:

Movies S1 to S3

www.pnas.org/cgi/doi/10.1073/pnas.2011780118

Supplementary Information Text

SI Materials and Methods

Cell culture. Undifferentiated H9 hESCs (WiCell) and their derivatives were cultured as previously described (18). Briefly, cells were grown on Matrigel (Corning, catalog number 356231)-coated plates in TeSR-E8 medium (Stem cell Technologies, 5990) at 37°C in a 5% CO_2 incubator. The culture medium was refreshed every day, and cells were conventionally passaged once a week. Cells were dissociated using 0.5 μM EDTA solution (Gibco, AM9261) and passaged to Matrigel-coated plates in TeSR-E8 supplemented with 10 μM Y-27632 (Selleck, S1049) to maintain pluripotency. Cell morphology was recorded using an inverted fluorescence microscope (ZEISS). Y79 cell lines were obtained from ATCC (HTB-18) and cultured in complete RPMI medium (RPMI 1640 with 20% fetal bovine serum, ATCC) at 37°C in a 5% CO_2 incubator.

CRISPR/Cas9-mediated genome editing. The *RB1*$^{-/-}$ hESCs was generated using CRISPR/Cas9 technology. Briefly, a sgRNA (forward: CACCGCGGTGGCGGCCGTTTTTCGG, and reverse: AAACCCGAAAAACGGCCGCCACCGC) targeting exon 1 of *RB1* was cloned into pX330-U6-Chimeric_BB-CBh-hSpCas9-2A-Puro (Addgene, 42230) to generate the CRISPR/Cas9 guide-carrying plasmids (49). hESCs were nucleofected with the constructed guide-carrying plasmids and selected with 2 μg/mL puromycin. Once single, stable transfectants were generated, they were isolated, cultured on Matrigel-coated plates. For detection of positive *RB1*$^{-/-}$ clones, the following primers were used: forward: TTTTCTCAGGGGACGTTGAAA, reverse: TCTGATGGACGCTCGCAA.

Karyotype analysis. Cells were treated with 0.1μg/mL colcemid (Gibco, 15212) at 37°C for 2 h, trypsinized, resuspended and incubated in 0.075 M potassium chloride for 15 min at 37°C, fixed with 3:1 methanol:acetic acid, and then dropped onto slides to spread the chromosomes. The chromosomes were visualized by Giemsa (Servicebio) staining.

Flow cytometry. Cells were washed with PBS and carefully trypsinized using Accutase, followed by several washes with PBS. Organoids were carefully dissociated into a single-cell suspension using 0.25%

trypsin-EDTA (Gibco, 25200-056). The single cells were resuspended in media and then stained with antibodies in PEB (PBS containing 0.5% BSA and 2 mM EDTA) buffer for 30 min at 4°C. The following antibodies were used: Alexa Fluor 488 Mouse anti-Oct3/4 (1:100, BD Biosciences, 560253), Alexa Fluor 647 Mouse anti-Ki-67(1:100, BD Biosciences, 558615). The cells were filtered through 100 μm nylon mesh and then analyzed for fluorescence by FACSCanto II (Becton Dickinson).

Cell cycle analysis. hESCs were carefully dissociated into single-cell suspensions using Accutase solution, washed twice with PBS, and then fixed overnight with cold 70% ethanol. Fixed cells were washed twice with PBS, followed by RNase (100 μg/mL, Sigma, R6148) treatment and propidium iodide (50 μg/mL, Sigma, P4170) staining for 30 min at 37°C. Approximately 1×10^6 cells were analyzed using a FACSCanto II (Becton Dickinson) to determine the cell cycle distribution pattern. The percentages of cells in the G1, S, and G2/M phases of the cell cycle were analyzed using ModFit 4.1 (Verity Software House).

RNA sequencing and analysis. Total RNA for each sample was isolated with TRIzol reagent and purified using the RNeasy Mini Kit (Qiagen, 74104) according to the manufacturer's instructions. RNA quality and quantity were assessed using a NanoDrop 2000, Agilent 2100 Bioanalyzer and Agilent RNA 6000 Nano Kit (Agilent Technologies, 5067-1511). RNA library construction and RNA Seq were performed by the Annoroad Gene Technology. Sequencing libraries were generated using NEB Next Ultra RNA Library Prep Kit for Illumina (NEB, E7530S), and library clustering was performed using HiSeq PE Cluster Kit v4-cBot-HS (Illumina, PE-401-4001) following the manufacturer's recommendations. After cluster generation, the libraries were sequenced on an Illumina platform and 150 bp paired-end reads were generated. The initial data analysis was performed on BMKCloud (http://www.biocloud.net/).

Single-cell RNA sequencing and analysis. Organoids were washed with PBS and carefully trypsinized in dissociation solution (2.4 mL 0.25% Trypsin-EDTA supplemented with 1.6 mL Accumax (Stem Cell Technologies, 07921) and 0.05 mg/mL DNase I (Roche, 11284932001) and incubated at 37°C in a 5% CO_2/40% O_2 incubator for 1 h. The cell suspension was then centrifuged for 5 min at 300 RCF, and the resuspended to prepare a suitable cell concentration of 700~1,200 cells/μL. Cells were loaded onto the 10x Chromium Single Cell Platform as described in the manufacturer's protocol. Samples were processed

(including generation of Gel Bead in Emulsion & Thermal cycling, Post Cycling Cleanup & cDNA Amplication, and Library Preparation & Quantification) following the manufacturer's protocol and sequenced on an Illumina X-ten instrument using 150-base-pair paired-end reads.

Raw 10x Genomics data were processed with the standard Cell Ranger pipeline (v3.0.2). Mapping to the GRCh38 human genome, quality control and read counting of Ensembl genes was performed to generate a single cell gene count matrix. Normalization, variance estimation, dimensionality reduction and clustering of single cells were performed by the monocle R package (v2.10.1). We set monocle to use the negative binomial distribution with fixed variance in downstream statistical tests and estimated size factors and dispersion. Genes with a minimum expression value of 0.5 that were detected in at least 10 cells were retained for subsequent analyses. There were 9,665 and 12,218 cells covering 19,997 genes in hRBO and hRO, respectively. On average, we detected ~1,500 genes per cell.

Principal component analysis was conducted to effectively focus on the more interesting biological variations. We further reduced the data into two dimensions using t-Distributed Stochastic Neighbour Embedding (tSNE). Cells were then grouped by density peak clustering, which is an efficient and highly scalable one-step clustering algorithm. The highly specific cell type marker genes were identified by Seurat (v3.0.2), which performs differential gene expression testing for each cluster and combines the p-values using meta-analysis methods. We explored these marker genes for each cluster and used them to annotate our clusters as specific cell types. Finally, we used Monocle2 to order cells according to a pseudotime. For ordering cells, we chose the differentially expressed genes across clusters ($q<0.05$) to define a cell's progress. Dimensionality reduction was carried out using the DDRTree method.

Whole-genome bisulfite sequencing (WGBS). Genomic DNA was isolated from each sample using a DNeasy Blood & Tissue Kit (QIAGEN, 69504) according to the manufacturer's protocol. DNA was quantified using NanoDrop 2000 and Qubit 2.0 Fluorometer. Genomic DNA (1 μg) was used to construct the WGBS library. Bisulfite conversion of genomic DNA was performed using the EZ DNA Methylation-Gold Kit (Zymo Research, D5005) according to the manufacturer's recommendation. Bisulfite-converted

DNA was subjected to processing as described and then sequencing (PE125/PE150) on an Illumina HiSeq platform.

The raw reads of WGBS data were trimmed by trim_galore (v0.5.0), and then mapped to GRCh38 (human) using Bismark (v0.18.2) with default parameters. We extracted the methylated CpGs with Bismark methylation extractor script. The number of converted and unconverted reads, total coverage and fractional methylation at each individual CpG were reported. Only CpG sites covered by five or more reads were retained for further analysis.

The global analysis of DNA methylation status between hRO and hRBO was performed using SMART2 software, an entropy-based framework used to detect DMRs. To strictly identify high-confidence aberrant methylation associated with Rb pathogenesis, we required that significant DMRs had adjusted p-values less than 0.01 as well as the absolute values of mean methylation differences greater than 0.25. Differentially methylated genes were visualized using EnhancedVolcano (v1.0.1) (Publication-ready volcano plots with enhanced coloring and labeling). For simplification, if multiple DMRs are simultaneously associated with the same gene, we choose the DMR with the maximum absolute methylation differences to represent the status of aberrant methylation of the target gene. The putative target genes of DMRs and their biological functions were determined by GREAT tools. The CpG island shore is defined as +/- 2 kb regions centred on CpG island, which is for the genomic element analysis, annotation files of GRCh38 were downloaded from Ensembl (http://ensembl.org/). The genomic elements including exon, intron, intergenic, and CGI regions were downloaded from the UCSC table browser, the overlap analysis between genomic elements and DMRs were calculated using software BEDTOOLS.

Xenografts. All procedures were performed under ethical animal licence protocols and approved by local authorities (Laboratory Animal Ethics Committee of Wenzhou Medical University). Most of the cells used for xenograft were excessively proliferating Rb-like cells that have migrated out of hRBOs and suspended in culture medium. A small number of supplementary cells for xenograft were isolated from hRBOs, which were washed with PBS and carefully trypsinized using 0.25% Trypsin-EDTA supplemented with 0.05 mg/mL DNaseI at 37 °C for 6-8 min. 2 μL of the cell suspension (50,000-80,000 cells/μL) was injected into

the subretinal space or vitreous cavity. For subretinal space or vitreous cavity injection, 6-week old immunodeficient NOD-*Prkdc*^{scid}*IL2rg*^{em2}/SMOC (NSG) mice (Shanghai Model Organisms) were first anaesthetized with an intraperitoneal injection of sodium pentobarbital (40 mg/kg, Sigma, P3761), and the pupils were then dilated with a drop of 2.5% phenylephrine hydrochloride solution, after which a drop of topical anaesthetic proparacaine hydrochloride (0.5%) was applied. Injections were performed using a Hamilton syringe with a 33-gauge needle under a surgical microscope. Mice were sacrificed 2 months after xenograft, and some tumor-bearing eyes were extracted for H&E staining, while the remaining eyes were kept for immunocytochemistry and TEM morphology analysis.

Intraocular imaging. After xenograft implantation, the development of retinal tumor was monitored by intraocular imaging using fundus photography and OCT. On the day of imaging, mice were anaesthetized with an intraperitoneal injection of sodium pentobarbital. Pupils were immediately dilated with a drop of 1% tropicamide, followed by topical application of ofloxacin eye ointment to prevent drying of the cornea. Then, fundus photography and OCT-imaging were completed using a Micron IV Retinal Imaging Microscope (Phoenix Research Labs).

Immunocytochemistry and H&E staining. Organoids were fixed in 4% paraformaldehyde (PFA, Beyotime, P0098) at 4°C for 60 min, embedded in NEG-50 frozen section medium (Thermo, 6502), and then cryosectioned at 12-16 μm on slides using a Leica cryostat. Sections were subjected to immunocytochemistry or storage at -80°C. Tissues were processed for cryosections using standard protocols with minor modifications (50). Briefly, tissues were dissected and post fixed in 4% PFA for 1 h followed by cryoprotection with 30% sucrose solution overnight, embedded in NEG-50, and then cryosectioned at 12-16 μm. Monolayer cells were fixed with 4% PFA for 15 min. For immunocytochemistry, sections and cells were first blocked and permeabilized in 4% BSA (Beyotime, ST023) supplemented with 0.5% Triton X-100 (Sangon, 600198-0500) for 1 h at room temperature and then stained with primary antibodies at 4°C overnight. After primary antibody staining, the sections and cells were then rinsed three times with PBS and subsequently incubated with secondary antibodies for 1 h at room temperature in the dark. After removal of the secondary antibody, the nuclei were stained with

300 nM DAPI stain solution (Thermo, D1306) for 5 min. Finally, the stained cells were visualized by confocal microscopy (Leica). For H&E staining, sections were stained with Hematoxylin and Eosin Staining Kit (Beyotime, C0105) and scanned using ZEN 2012 (blue edition) scanning system (ZEISS). Antibodies are described in *SI Appendix*, Table S2.

Western blot analysis. Western blot analysis was performed conventionally. Briefly, cells were washed twice with PBS and lysed in M-PER Mammalian Protein Extraction Reagent (Thermo, 78501) containing 1×Halt Protease Inhibitor Cocktail (Thermo, 87785). Equal amounts (20-40 μg) of total protein were boiled, electrophoresed on 12% SDS-polyacrylamide gels and electroblotted onto PVDF membranes (Millipore). Membranes were blocked for 1 h with 5% fat-free milk solution or 5% BSA, probed with primary antibodies (*SI Appendix*, Table S2) overnight at 4°C, and then incubated with secondary antibodies at room temperature for 2 h. Images were recorded using the Li-Cor Odyssey 9120 Infrared Imaging System (LICOR).

Transmission electron microscopy (TEM) analysis. For TEM analysis, organoids and tissues were fixed in 2.5% EM-grade glutaraldehyde (Servicebio) for 2-4 h at 4°C, washed with 0.1 M phosphate buffer (pH 7.4), postfixed in 1% osmium tetroxide for 2-4 h at 4°C, washed and then dehydrated in an ethanol series (50-100%) to a final rinse in 100% acetone, followed by 2 h incubations in 1:1 acetone/Pon 812 (SPI) and overnight incubation in 1:2 acetone/Pon 812, The samples were embedded in Pon 812, polymerized for 48 h at 60°C, and then sectioned (60-80 nm) with a diamond knife (Daitome). Sections were stained with 2% uranyl acetate followed by lead citrate, and visualized using a HT7700 transmission electron microscope (HITACHI).

Optical coherence tomography imaging of live organoids. Deep optical coherence tomography (dOCT) imaging of live organoids was performed using a commercial Cell iMager Estier system

(SCREEN) according to the manufacturer's protocols. Organoids were imaged while cultured with medium in dishes placed in the device's imaging plane.

Chemotherapeutic drug testing on human Rb organoids. Rb organoids were generated as described above and treated with chemotherapy drugs at day 60 (stage I, early intervention) or 90 (stage II, conventional therapy). After drug treatment, organoids were collected at day 120 and then subjected to flow cytometry and immunostaining analysis. Chemotherapy drugs including vincristine (final concentration: 5 nM; Selleck, S1241), etoposide (0.5 μM; J&K, 320523), carboplatin (10 μM; Selleck, S1215), topotecan (10 nM; J&K, T2705), rapamycin (10 μM; Selleck, S1039), R406 (5 μM; Selleck, S2194) and BAY-61-3606 (5 μM; MedChemExpress, HY-14985) were applied, and DMSO was used as the control.

Statistical analyses. All experiments were performed at least three times independently. The results are expressed as mean ± SD. Data were analyzed by unpaired two-tailed Student's t-test for comparison of two groups, and by one-way ANOVA with Tukey's test or Dunnett's multiple comparisons test for comparisons of multiple groups. All analyses were performed using SPSS Statistics 19.0 software. *P*-values < 0.05 were considered significant.

Figure S1

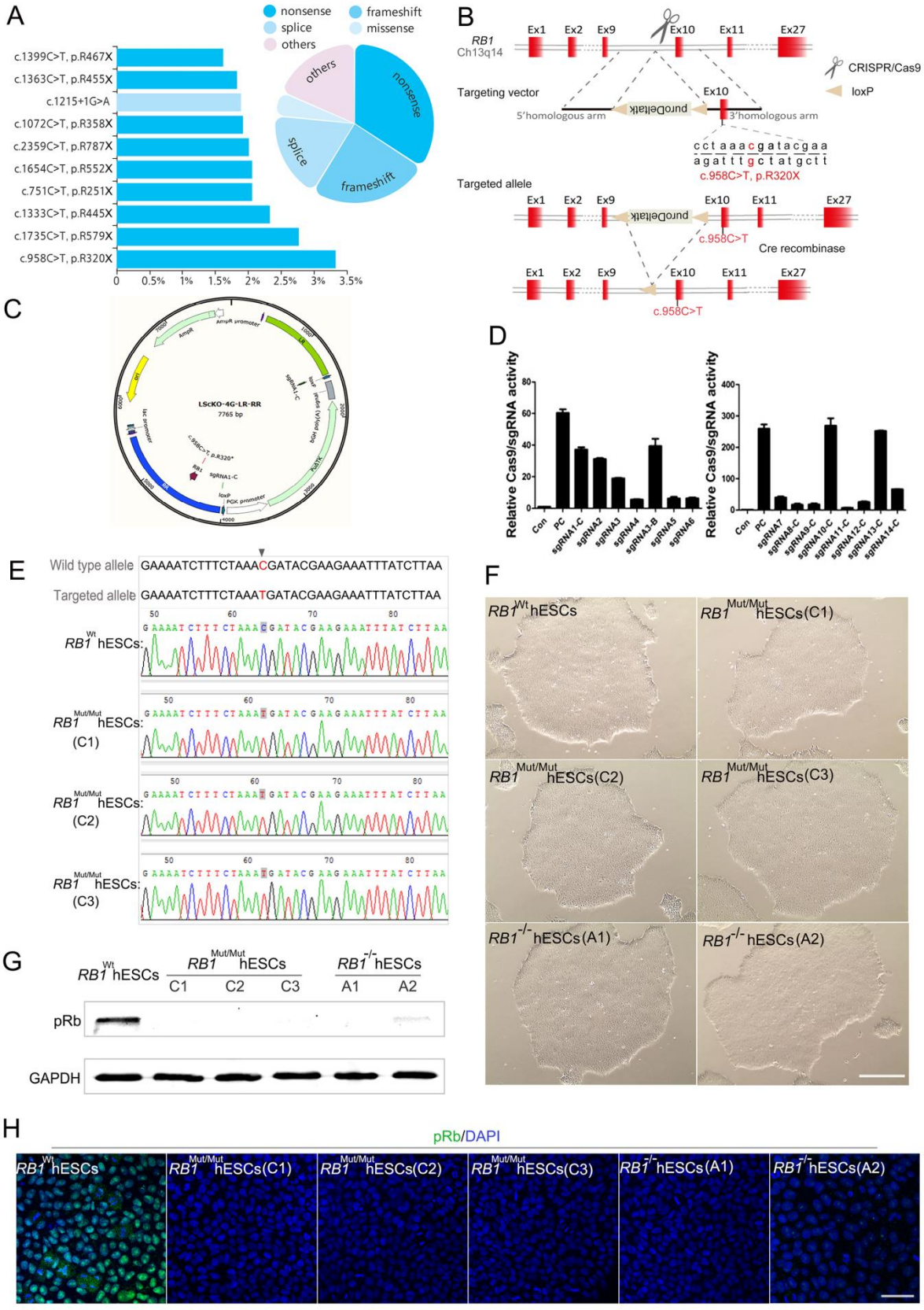
A
nonsense
frameshift
splice
missense
others
c.1399C>T, p.R467X
c.1363C>T, p.R455X
c.1215+1G>A
c.1072C>T, p.R358X
c.2359C>T, p.R787X
c.1654C>T, p.R552X
c.751C>T, p.R251X
c.1333C>T, p.R445X
c.1735C>T, p.R579X
c.958C>T, p.R320X
0 0.5% 1% 1.5% 2% 2.5% 3% 3.5%
B
RB1
Ch13q14
Ex1 Ex2 Ex9 Ex10 Ex11 Ex27
CRISPR/Cas9
loxP
Targeting vector
5'homologous arm
puroDeltatk
3'homologous arm
c c t a a a c g a t a c g a a
a g a t t t g c t a t g c t t
c.958C>T, p.R320X
Targeted allele
Cre recombinase
c.958C>T
C
LScKO-4G-LR-RR
7765 bp
D
Relative Cas9/sgRNA activity
Con PC sgRNA1-C sgRNA2 sgRNA3 sgRNA4 sgRNA3-B sgRNA5 sgRNA6
Con PC sgRNA7 sgRNA8-C sgRNA9-C sgRNA10-C sgRNA11-C sgRNA12-C sgRNA13-C sgRNA14-C
E
Wild type allele GAAAATCTTTCTAAACGATACGAAGAAATTTATCTTAA
Targeted allele GAAAATCTTTCTAAATGATACGAAGAAATTTATCTTAA
RB1 Wt hESCs:
RB1 Mut/Mut hESCs: (C1)
RB1 Mut/Mut hESCs: (C2)
RB1 Mut/Mut hESCs: (C3)
F
RB1 Wt hESCs
RB1 Mut/Mut hESCs(C1)
RB1 Mut/Mut hESCs(C2)
RB1 Mut/Mut hESCs(C3)
RB1 -/- hESCs(A1)
RB1 -/- hESCs(A2)
G
RB1 Wt hESCs
RB1 Mut/Mut hESCs
C1 C2 C3
RB1 -/- hESCs
A1 A2
pRb
GAPDH
H
pRb/DAPI
RB1 Wt hESCs
RB1 Mut/Mut hESCs(C1)
RB1 Mut/Mut hESCs(C2)
RB1 Mut/Mut hESCs(C3)
RB1 -/- hESCs(A1)
RB1 -/- hESCs(A2)

Figure S1. Generation of *RB1*$^{Mut/Mut}$ and *RB1*$^{-/-}$ hESCs. (**A**) Top10 of *RB1* point mutations in previously reported cases (left); Distribution of total *RB1* mutations by type (right). (**B**) Targeting strategy for the generation of *RB1*$^{Mut/Mut}$ hESCs including mutation knock-in and resistance gene remove. (**C**) Sequence map for LScKO-4G-*RB1* targeting vector. (**D**) Detection of CRISPR sgRNA activity. (**E**) Sequences of targeted loci in *RB1*$^{Mut/Mut}$ hESCs. (**F**) Bright field images of *RB1*$^{Mut/Mut}$ and *RB1*$^{-/-}$ hESC colonies. Scale bar, 400 μm. (**G**) Western blot analysis for expression of pRb in *RB1*$^{Mut/Mut}$ and *RB1*$^{-/-}$ hESCs. (**H**) Immunostaining analysis for pRB in *RB1*$^{Mut/Mut}$ and *RB1*$^{-/-}$ hESC lines. Scale bars, 50 μm.

Figure S2

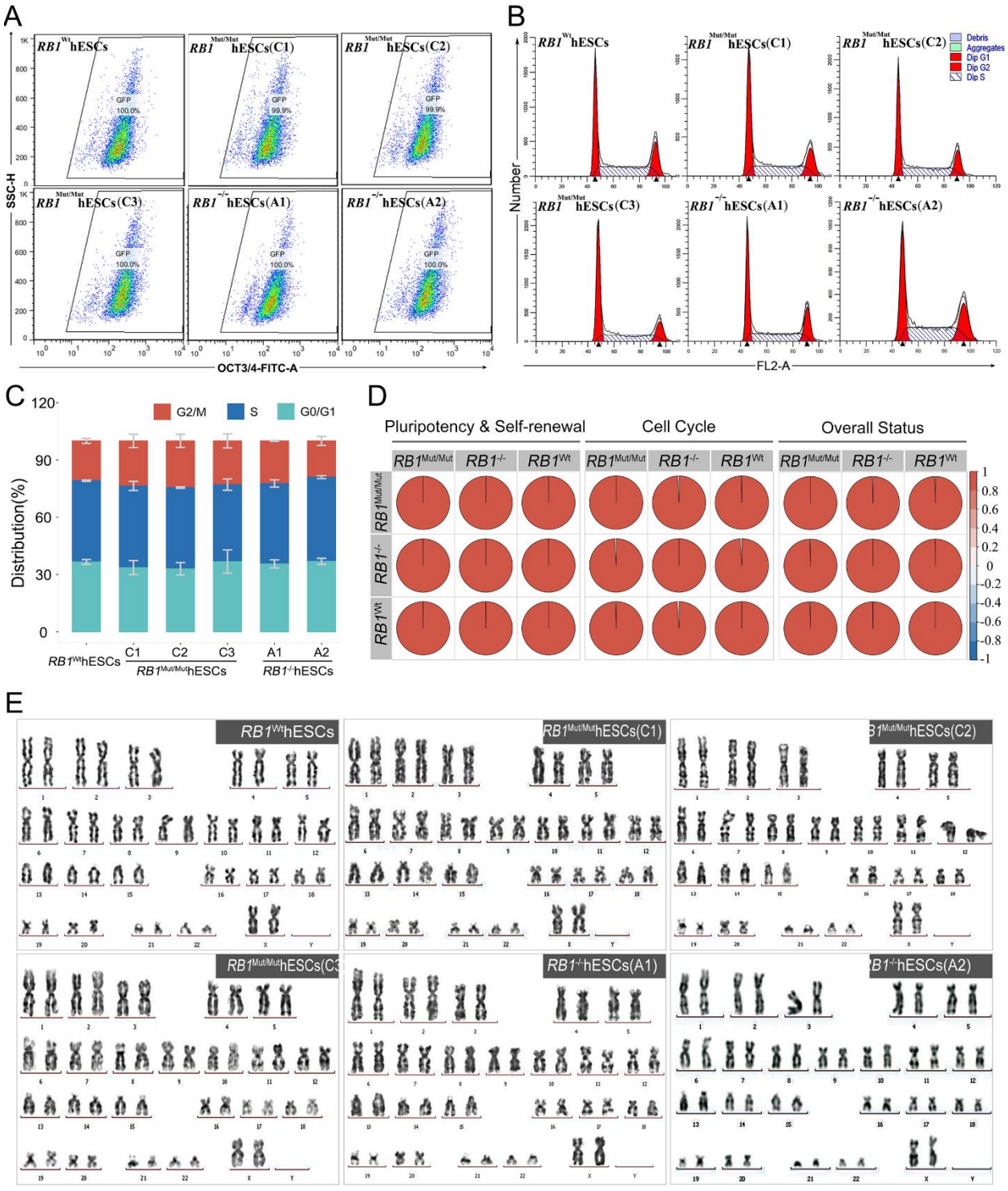
A
B
C
D
E
SSC-H
OCT3/4-FITC-A
Number
FL2-A
Debris
Aggregates
Dip G1
Dip G2
Dip S
G2/M
S
G0/G1
Distribution(%)
Pluripotency & Self-renewal
Cell Cycle
Overall Status

Figure S2. *RB1*$^{Mut/Mut}$ and *RB1*$^{-/-}$ hESC lines sustain the primordial state. (**A**) Flow cytometry analysis of OCT3/4 positive cells in *RB1*$^{Mut/Mut}$, *RB1*$^{-/-}$ and wild-type hESCs. (**B**) Cell cycle analysis of *RB1*$^{Mut/Mut}$, *RB1*$^{-/-}$ and wild-type hESCs. (**C**) Relative percentage within each cell cycle phase is represented. (**D**) Correlation heatmaps of the expression of pluripotency & self-renewal, cell cycle, and overall status associated genes in *RB1*$^{Mut/Mut}$, *RB1*$^{-/-}$ and wild-type hESCs base on RNA-Seq data. (**E**) Karyotype analysis of *RB1*$^{Mut/Mut}$, *RB1*$^{-/-}$ and wild-type hESCs.

Figure S3

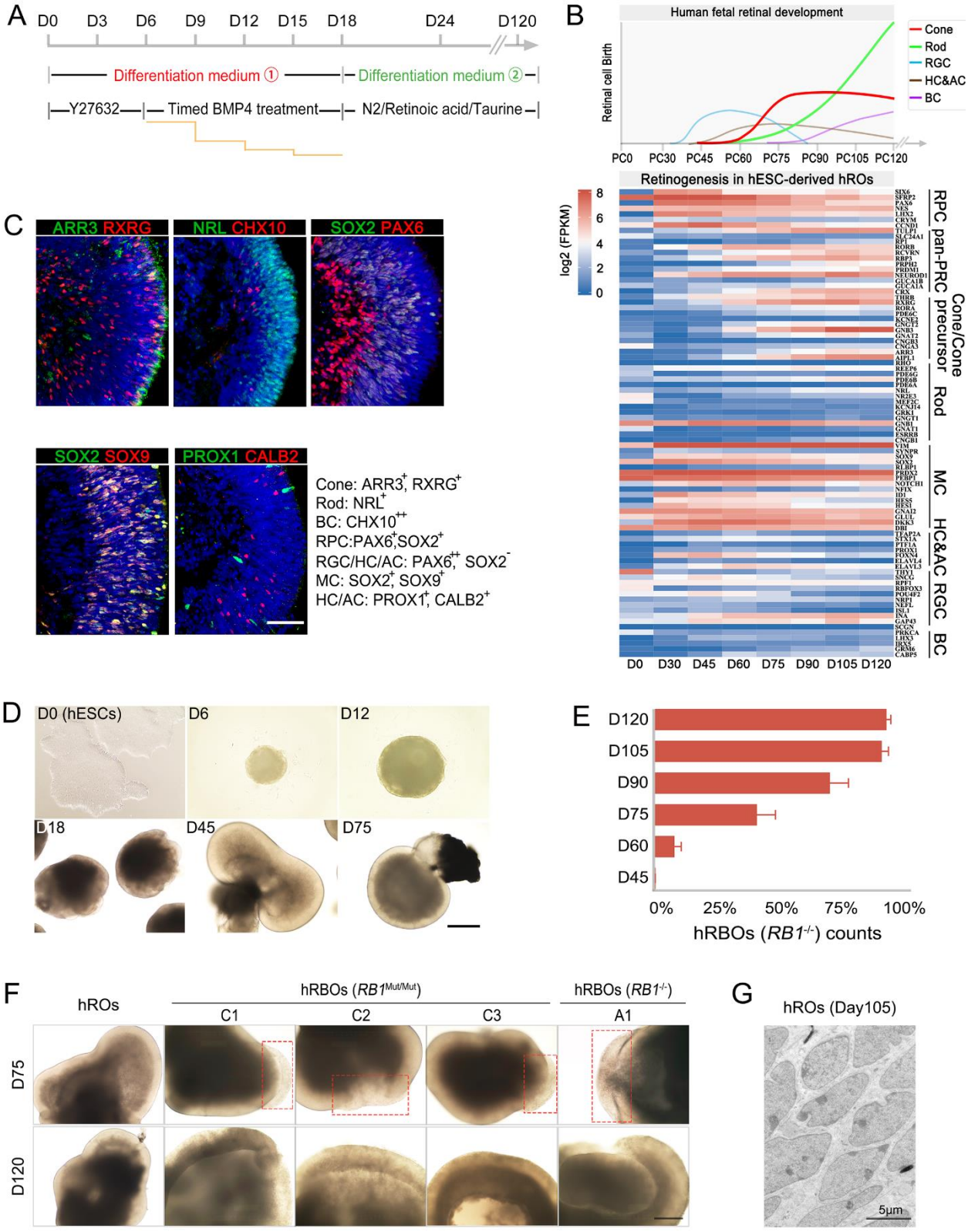
A
D0 D3 D6 D9 D12 D15 D18 D24 D120
Differentiation medium ①
Differentiation medium ②
Y27632
Timed BMP4 treatment
N2/Retinoic acid/Taurine
B
Human fetal retinal development
Retinal cell Birth
Cone
Rod
RGC
HC&AC
BC
PC0 PC30 PC45 PC60 PC75 PC90 PC105 PC120
Retinogenesis in hESC-derived hROs
log2 (FPKM)
8
6
4
2
0
RPC
pan-PRC
Cone/Cone precursor
Rod
MC
HC&AC
RGC
BC
D0 D30 D45 D60 D75 D90 D105 D120
C
ARR3 RXRG
NRL CHX10
SOX2 PAX6
SOX2 SOX9
PROX1 CALB2
Cone: ARR3+, RXRG+
Rod: NRL+
BC: CHX10++
RPC:PAX6+,SOX2+
RGC/HC/AC: PAX6++, SOX2-
MC: SOX2+, SOX9+
HC/AC: PROX1+, CALB2+
D
D0 (hESCs)
D6
D12
D18
D45
D75
E
D120
D105
D90
D75
D60
D45
0% 25% 50% 75% 100%
hROBs (RB1-/-) counts
F
hROs
hRBOs (RB1Mut/Mut)
C1
C2
C3
hRBOs (RB1-/-)
A1
D75
D120
G
hROs (Day105)
5μm

Figure S3. Development of *RB1*$^{Mut/Mut}$ and *RB1*$^{-/-}$ hESC-derived hRBOs. (**A**) Stepwise culture strategy of retinal organoids derived from hESCs. (**B**) Retinal cell genesis at different organoid stages in hESC-derived hROs (bottom row); the relative numbers and developmental birth order of each retinal cell types *in vivo* are shown (top row) (26, 27). (**C**) Immunostaining of retinal cell type-specific proteins in day 105 hROs. Scale bar, 50 μm. (**D**) Representative bright-field images of hESC-derived hROs in different differentiation stages. Scale bar, 400 μm. (**E**) Quantification of *RB1*$^{-/-}$ hESC-derived organoids with tumor-like structures in different organoid stages. (**F**) Representative bright-field images of developing *RB1*$^{Mut/Mut}$ and *RB1*$^{-/-}$ hESC-derived hRBOs at day 75 and 120. Wild-type hESC-derived hROs were used as the control. Dashed lines denote the tumor-like structures. Scale bar, 400 μm. (**G**) Transmission electron micrograph of cells from day 105 hESC-derived normal hROs. Scale bar, 5 μm.

Figure S4

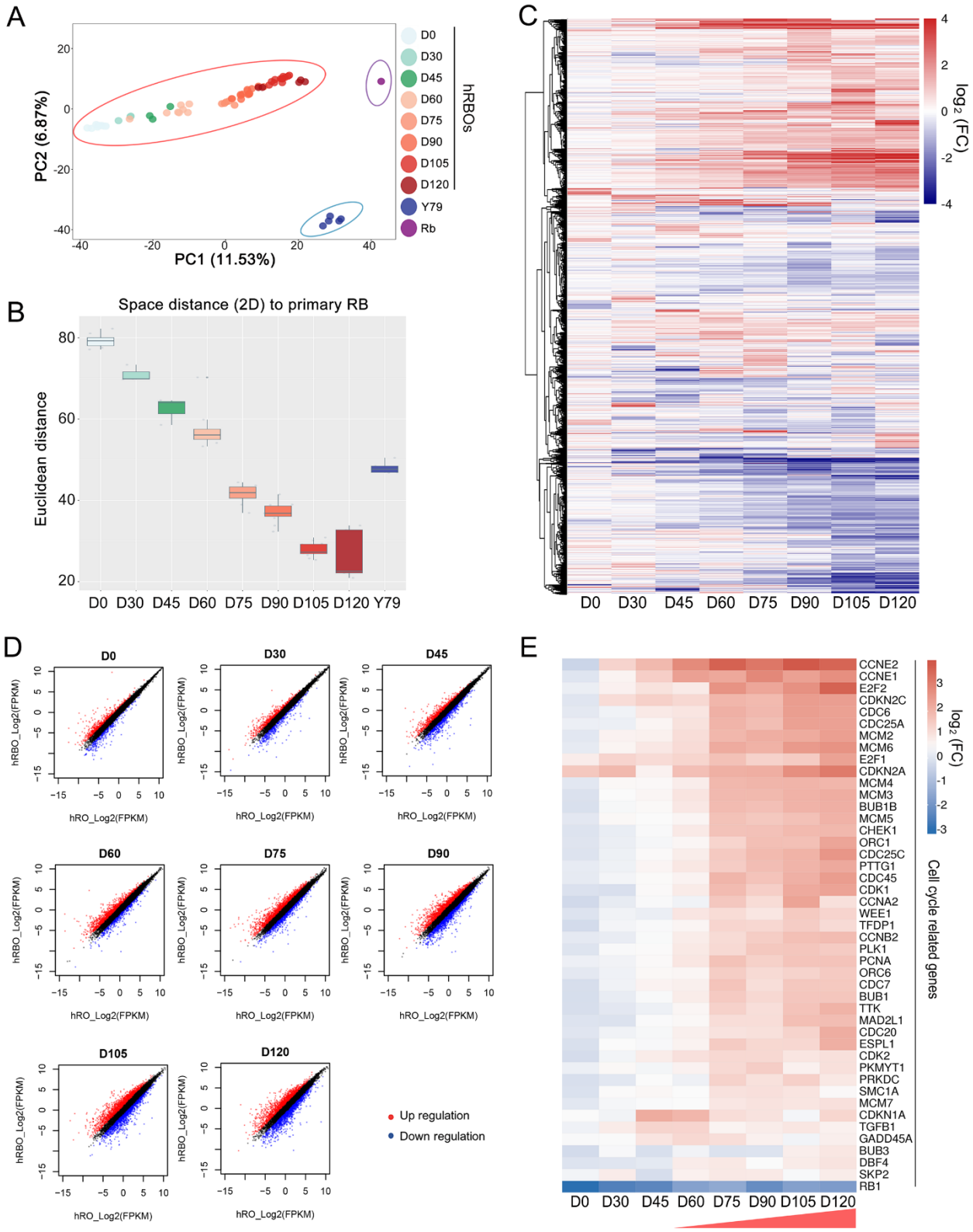
A
PC2 (6.87%)
PC1 (11.53%)
D0
D30
D45
D60
D75
D90
D105
D120
Y79
Rb
hRBOs
B
Space distance (2D) to primary RB
Euclidean distance
D0 D30 D45 D60 D75 D90 D105 D120 Y79
C
log2 (FC)
D0 D30 D45 D60 D75 D90 D105 D120
D
D0
D30
D45
D60
D75
D90
D105
D120
hRBO_Log2(FPKM)
hRO_Log2(FPKM)
Up regulation
Down regulation
E
CCNE2
CCNE1
E2F2
CDKN2C
CDC6
CDC25A
MCM2
MCM6
E2F1
CDKN2A
MCM4
MCM3
BUB1B
MCM5
CHEK1
ORC1
CDC25C
PTTG1
CDC45
CDK1
CCNA2
WEE1
TFDP1
CCNB2
PLK1
PCNA
ORC6
CDC7
BUB1
TTK
MAD2L1
CDC20
ESPL1
CDK2
PKMYT1
PRKDC
SMC1A
MCM7
CDKN1A
TGFB1
GADD45A
BUB3
DBF4
SKP2
RB1
Cell cycle related genes
log2 (FC)
D0 D30 D45 D60 D75 D90 D105 D120

Figure S4. Molecular characterization of hRBOs. (**A**) Principal-component analysis (PCA) of hRBOs at different organoid stages, Y79 cell line, and human primary Rb based on the expression of indicated genes correspond with those in Fig. 2*A*. Euclidean distance measurement between each sample and primary Rb in 2D PCA plot were also shown in (**B**). (**C**) Heatmap of all differentially expressed genes (FC>2) between the hRBOs and normal hROs across different organoid stages (days 0-120). (**D**) Scatterplots show the expressional alterations of all genes between the hRBOs and normal hROs at different organoid stages. The red and blue points represent the up- and down-regulated genes, respectively. (**E**) Heatmap showing the average $\log_2$-fold difference in the cell cycle related genes between the hRBOs and control hROs at different organoid stages.

Figure S5

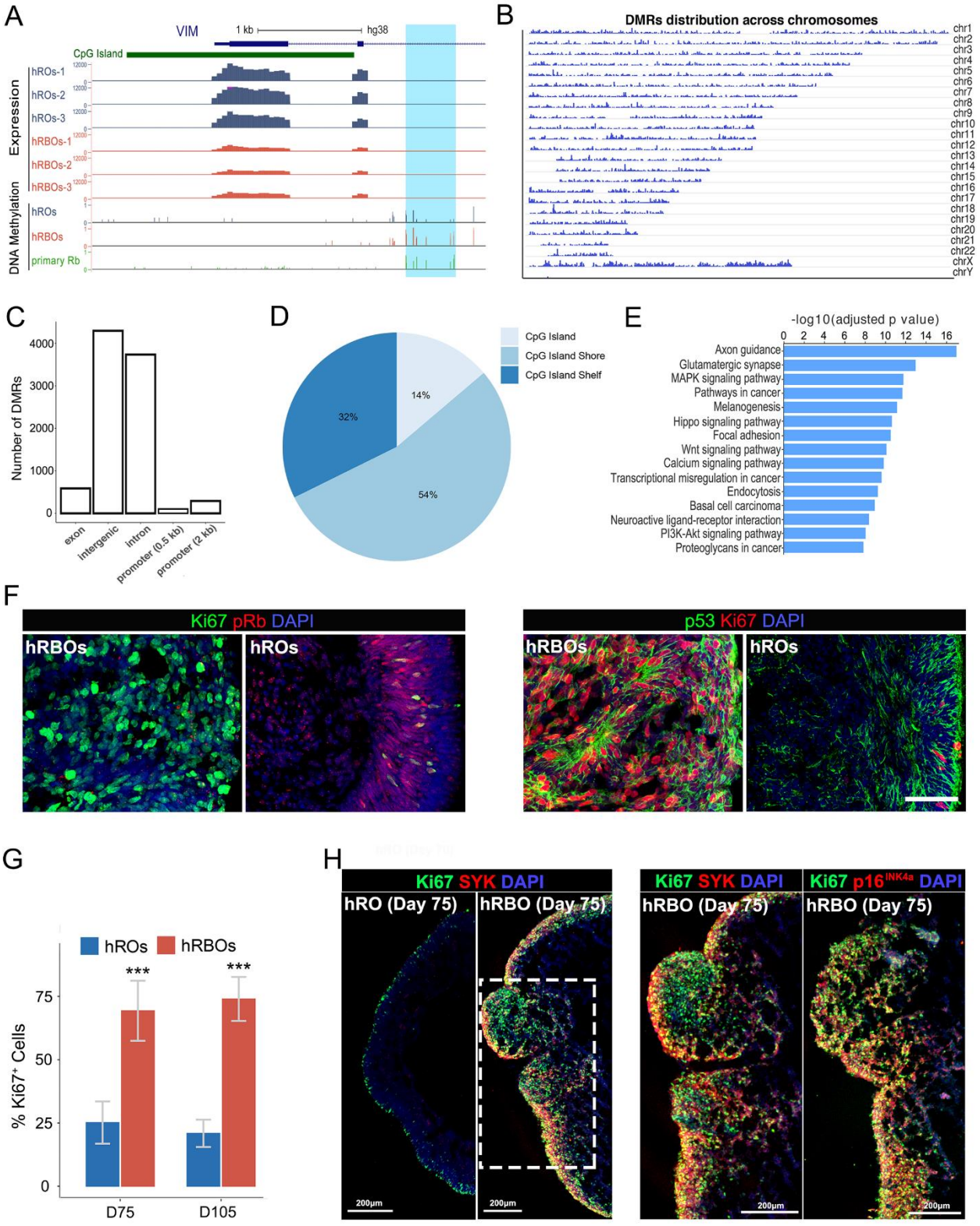
A
VIM
1 kb
hg38
CpG Island
Expression
hROs-1
hROs-2
hROs-3
hRBOs-1
hRBOs-2
hRBOs-3
DNA Methylation
hROs
hRBOs
primary Rb
B
DMRs distribution across chromosomes
chr1
chr2
chr3
chr4
chr5
chr6
chr7
chr8
chr9
chr10
chr11
chr12
chr13
chr14
chr15
chr16
chr17
chr18
chr19
chr20
chr21
chr22
chrX
chrY
C
Number of DMRs
4000
3000
2000
1000
0
exon
intergenic
intron
promoter (0.5 kb)
promoter (2 kb)
D
CpG Island
CpG Island Shore
CpG Island Shelf
14%
32%
54%
E
-log10(adjusted p value)
0 2 4 6 8 10 12 14 16
Axon guidance
Glutamatergic synapse
MAPK signaling pathway
Pathways in cancer
Melanogenesis
Hippo signaling pathway
Focal adhesion
Wnt signaling pathway
Calcium signaling pathway
Transcriptional misregulation in cancer
Endocytosis
Basal cell carcinoma
Neuroactive ligand-receptor interaction
PI3K-Akt signaling pathway
Proteoglycans in cancer
F
Ki67 pRb DAPI
hRBOs
hROs
p53 Ki67 DAPI
hRBOs
hROs
G
hROs
hRBOs
***
***
% Ki67⁺ Cells
75
50
25
0
D75
D105
H
Ki67 SYK DAPI
hRO (Day 75)
hRBO (Day 75)
200μm
200μm
Ki67 SYK DAPI
hRBO (Day 75)
200μm
Ki67 p16INK4a DAPI
hRBO (Day 75)
200μm

Figure S5. Tumorigenesis identification in hRBOs. (**A**) Genomic snapshots of RNA-seq and WGBS for *VIM* (a known low-expressed gene in primary Rb) in hRBOs and control hROs. Representative methylation level of *VIM* from human primary Rb sample is also shown. Enlarged view of the specific site is shown below. (**B**) The DMRs distribution across different chromosomes. (**C**) The overlap analysis between DRMs and different genomic elements. (**D**) The pie chat shows the distribution of DMRs against CGI, CGI shore, and CGI shelf. (**E**) KEGG analysis of DMRs associated genes and 15 significant pathways were showed. (**F**) Co-immunostaining of pRb and p53 with the proliferative marker Ki67 in day 105 hRBOs and control hROs. Scale bar, 50 μm. (**G**) Quantification of $Ki67^+$ cells in hROs and hRBOs at day 75 and 105 as analyzed by immunostaining. (**H**) Immunostaining of Rb signature genes Ki67 and SYK in hRBOs and hROs at day 75 (left). Co-immunostaining of Ki67 with SYK and $p16^{INK4a}$ and ARR3 in hRBOs at day 75 (right). Dashed lines denote the tumor-like structures. Scale bar, 200 μm.

Figure S6

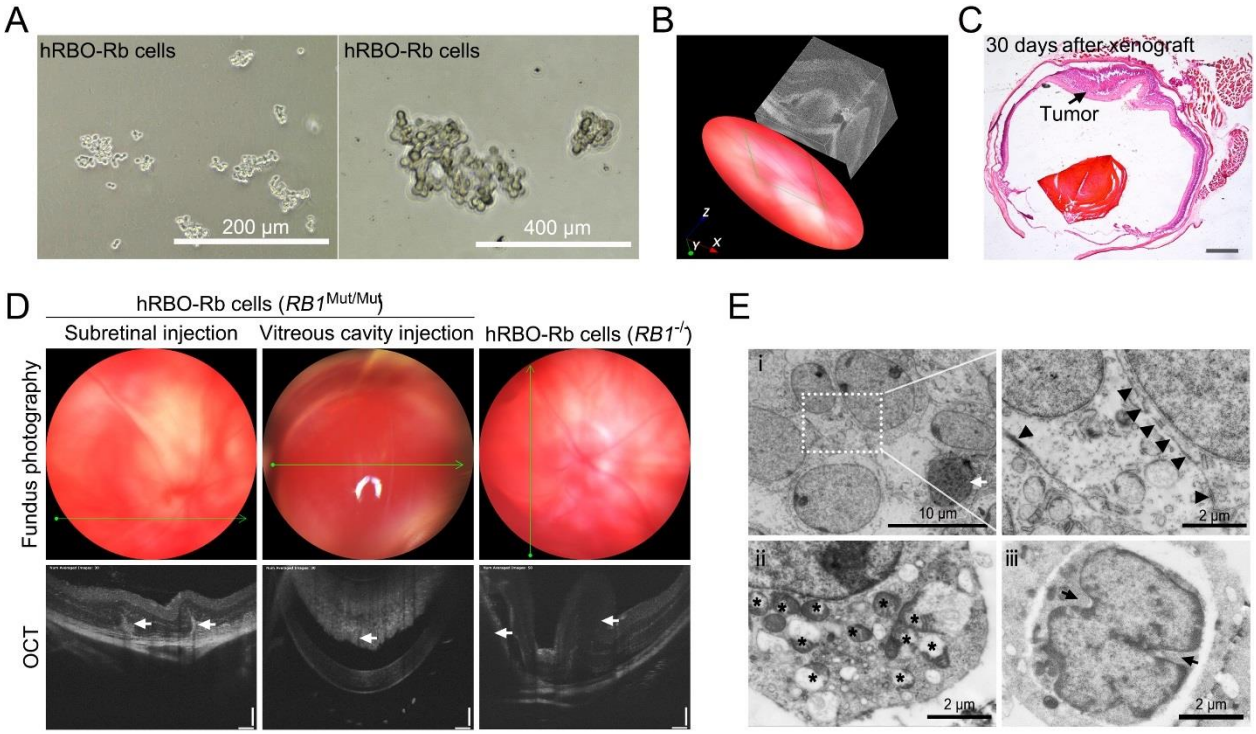

Figure S6. High tumorigenicity of hRBOs *in vivo*. (**A**) Representative bright-field image of hRBO-derived Rb cells cultured in suspension conditions. (**B**) Representative 3D imaging of Rb engraftments by OCT. (**C**) Representative H&E staining of hRBO-Rb cells engrafted eyes one month after subretinal injection. Scale bars, 200 μm. (**D**) Ophthalmic examination of mouse eyes after subretinal (left) or vitreous (middle) engraftment of *RB1*$^{Mut/Mut}$ or *RB1*$^{-/-}$ hRBO-Rb cells (right). Arrows indicate the viable Rb engraftments. (**E**) Representative transmission electron micrograph of Rb engraftments. (i) White arrow indicates a mitotic figure; Arrowheads indicate the structure of tight junction. Magnified view of the boxed region is shown in right. Abundant mitochondria (asterisks) and mitotically proliferating cell (black arrows) are shown in (ii) and (iii), respectively.

Figure S7

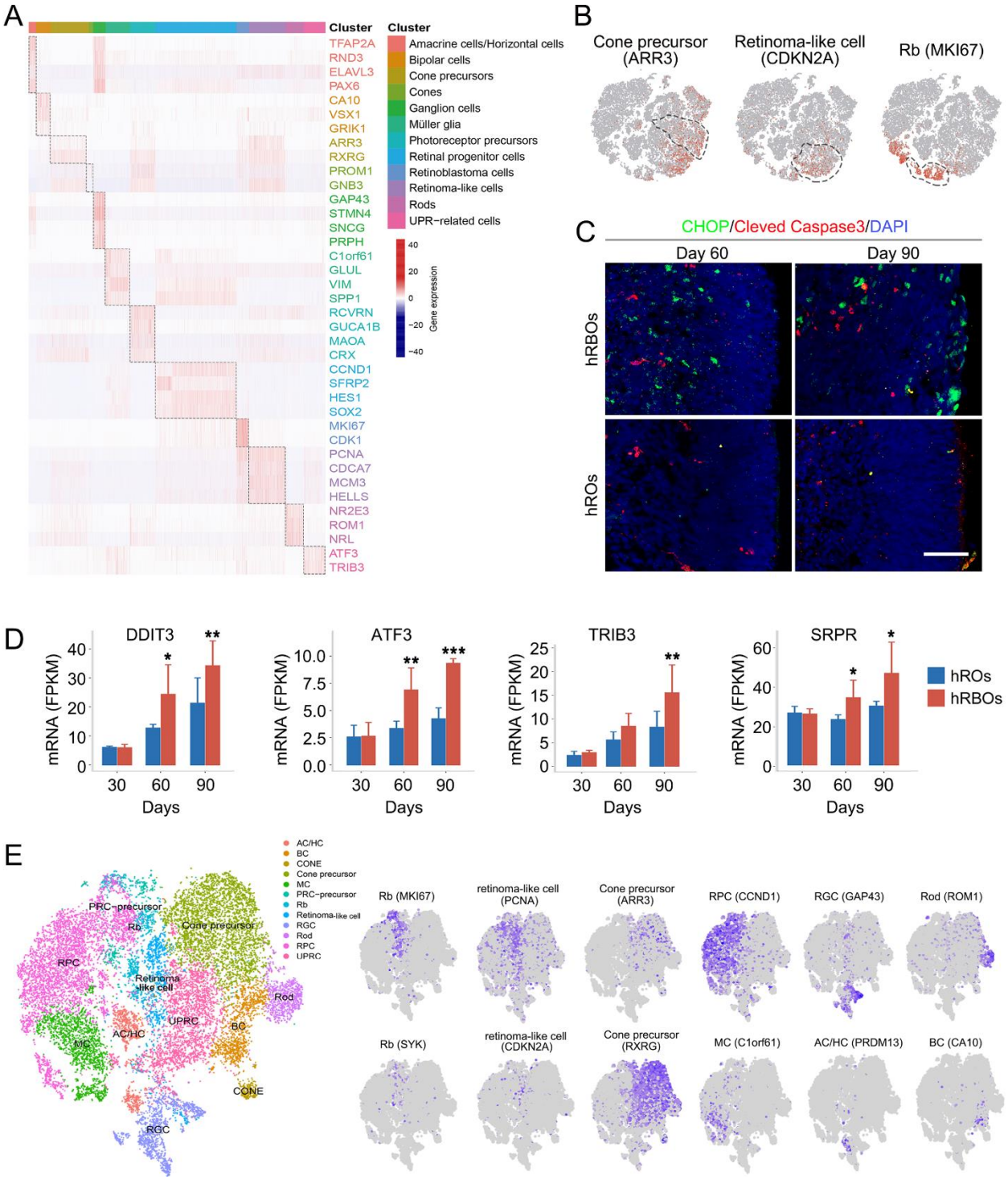
A
Cluster
Cluster
Amacrine cells/Horizontal cells
Bipolar cells
Cone precursors
Cones
Ganglion cells
Müller glia
Photoreceptor precursors
Retinal progenitor cells
Retinoblastoma cells
Retinoma-like cells
Rods
UPR−related cells
Gene expression
TFAP2A
RND3
ELAVL3
PAX6
CA10
VSX1
GRIK1
ARR3
RXRG
PROM1
GNB3
GAP43
STMN4
SNCG
PRPH
C1orf61
GLUL
VIM
SPP1
RCVRN
GUCA1B
MAOA
CRX
CCND1
SFRP2
HES1
SOX2
MKI67
CDK1
PCNA
CDCA7
MCM3
HELLS
NR2E3
ROM1
NRL
ATF3
TRIB3
B
Cone precursor (ARR3)
Retinoma-like cell (CDKN2A)
Rb (MKI67)
C
CHOP/Cleved Caspase3/DAPI
Day 60
Day 90
hRBOs
hROs
D
DDIT3
ATF3
TRIB3
SRPR
mRNA (FPKM)
Days
hROs
hRBOs
E
AC/HC
BC
CONE
Cone precursor
MC
PRC−precursor
Rb
Retinoma-like cell
RGC
Rod
RPC
UPRC
Rb (MKI67)
retinoma-like cell (PCNA)
Cone precursor (ARR3)
RPC (CCND1)
RGC (GAP43)
Rod (ROM1)
Rb (SYK)
retinoma-like cell (CDKN2A)
Cone precursor (RXRG)
MC (C1orf61)
AC/HC (PRDM13)
BC (CA10)

Figure S7. Single-cell transcriptomes from hRBOs reveal the cellular identity of Rb. (**A**) Heatmap shows the expression of key cell type-signature genes in each cell cluster. (**B**) Expression of representative marker gene for the cone precursor (*ARR3*), retinoma-like (*CDKN2A*) and Rb (*MKI67*) cell clusters on the tSNE map. Dashed lines denote the corresponding cell clusters. (**C**) Co-immunostaining of UPR related protein CHOP with the apoptosis marker cleaved caspase 3 in hRBOs and control hROs at day60 and 90. Scale bars, 50 μm. (**D**) Bar graphs showing the expression of UPR related genes, *DDIT3* (CHOP), *ATF3*, *TRIB3*, and *SRPR*, in hRBOs and control hROs. Data are shown as mean FPKM±SD from RNA-Seq data. (**E**) Single-cell RNA-seq analysis of hRBO and hRO after regressing out cell cycle scores. tSNE visualization of cells in 90-day-old hRBOs and control hROs profiled with each cell colored according to cell type annotations (left). Expression of marker genes for the main cell clusters on the tSNE map (right).

Figure S8

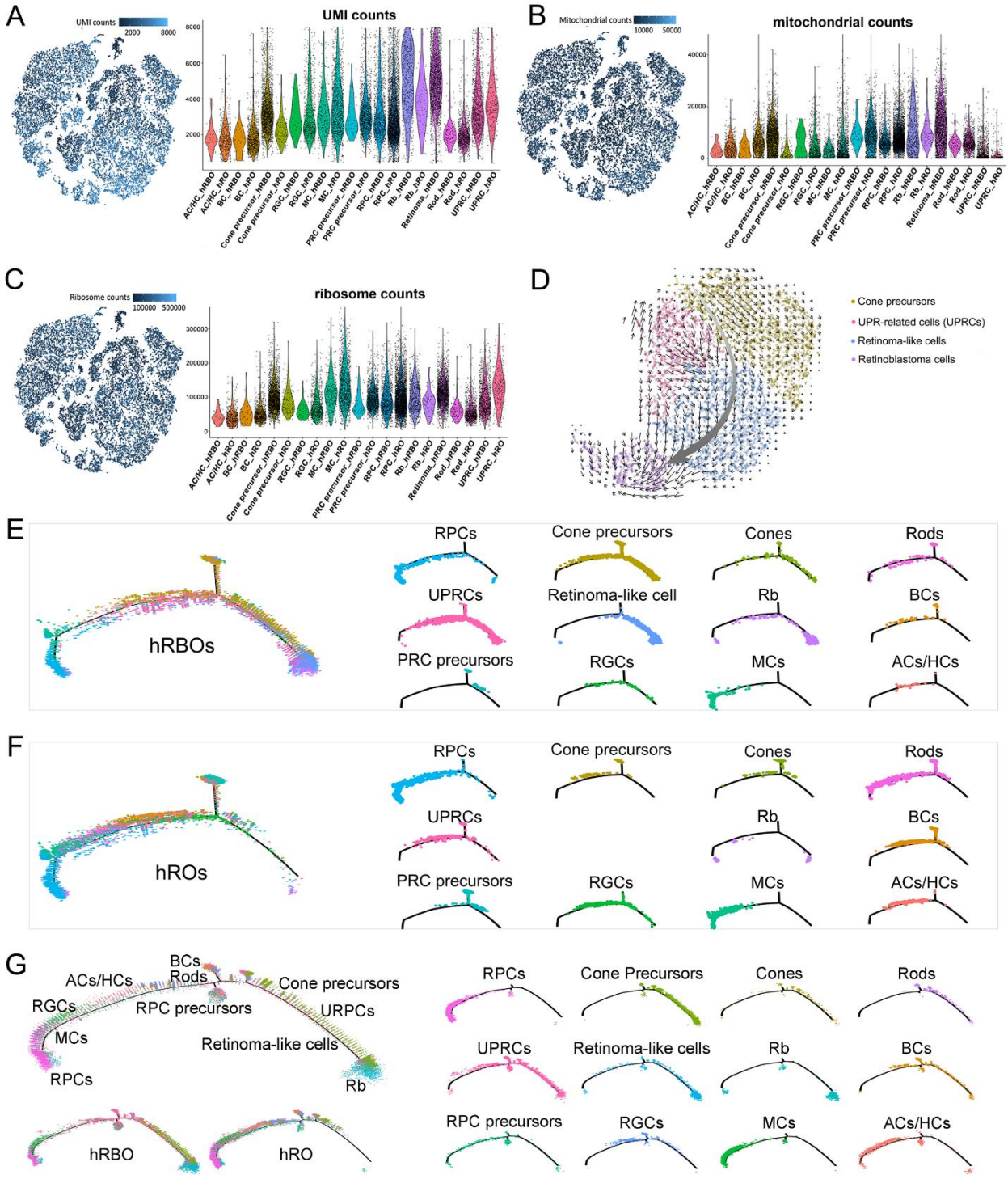
A
UMI counts
2000
8000
UMI counts
B
Mitochondrial counts
10000
50000
mitochondrial counts
C
Ribosome counts
100000
500000
ribosome counts
D
Cone precursors
UPR-related cells (UPRCs)
Retinoma-like cells
Retinoblastoma cells
E
hRBOs
RPCs
Cone precursors
Cones
Rods
UPRCs
Retinoma-like cell
Rb
BCs
PRC precursors
RGCs
MCs
ACs/HCs
F
hROs
RPCs
Cone precursors
Cones
Rods
UPRCs
Rb
BCs
PRC precursors
RGCs
MCs
ACs/HCs
G
ACs/HCs
BCs
Rods
Cone precursors
RGCs
RPC precursors
URPCs
MCs
Retinoma-like cells
RPCs
Rb
hRBO
hRO
RPCs
Cone Precursors
Cones
Rods
UPRCs
Retinoma-like cells
Rb
BCs
RPC precursors
RGCs
MCs
ACs/HCs

Figure S8. Trajectory analysis of single cells in hRBOs and control hROs. (**A**-**C**) Quality control for Single-cell RNA-seq analysis. Heat and violin plot of UMI (**A**), mitochondrial (**B**) and ribosome (**C**) counts for each sample. (**D**) RNA Velocity analysis showing the origin of Rb cells and inter-relationship of four main populations in hRBOs. The velocities are visualized on the pre-defined t-SNE plot from the Figure 4A. (**E**, **F**) Single-cell pseudotime trajectory analysis of each cell type from hRBOs and control hROs. (**G**) Single-cell pseudotime trajectory analysis of each cell type from hRBOs and control hROs after regressing out cell cycle scores.

Figure S9

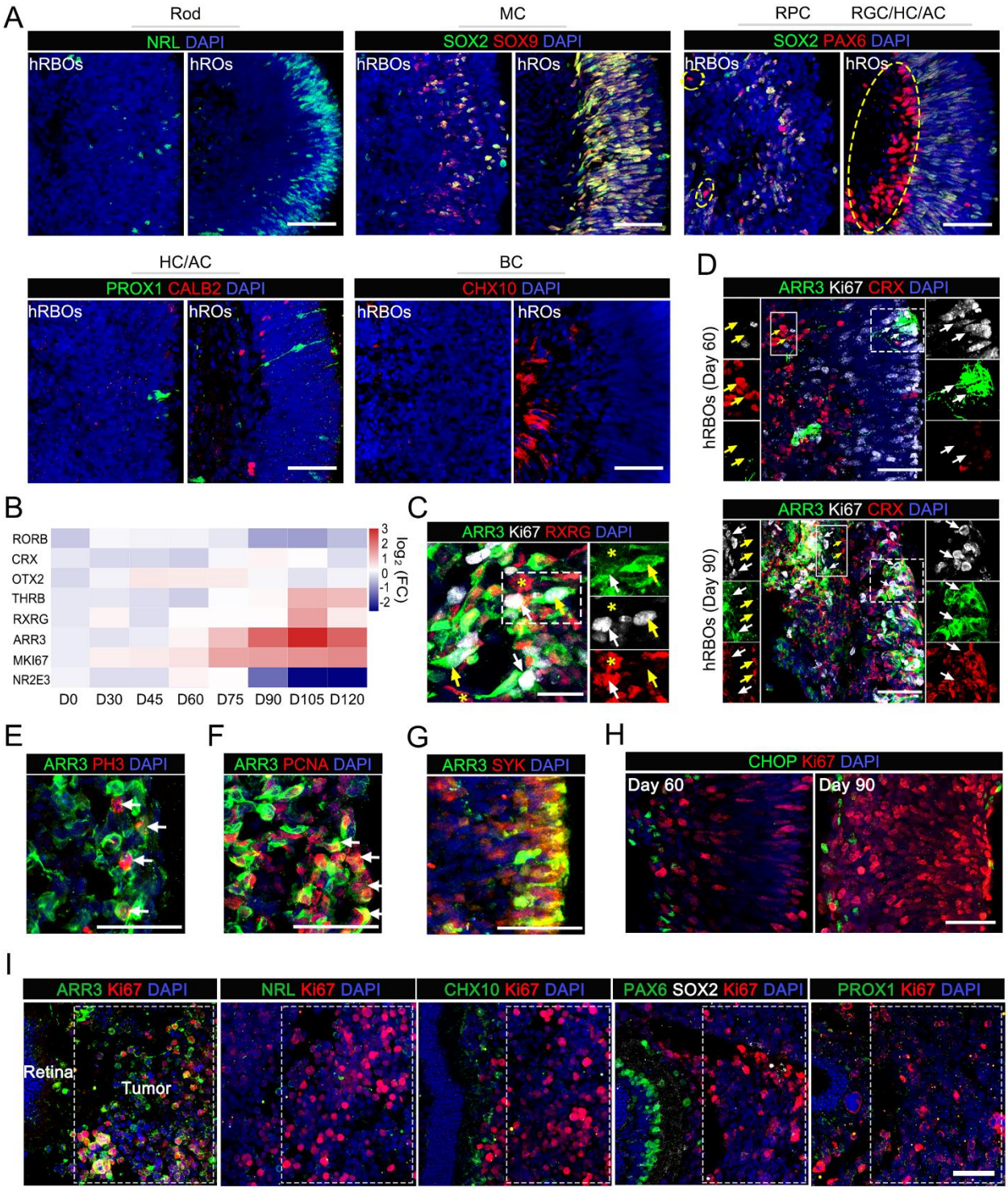
A
Rod
NRL DAPI
hRBOs
hROs
MC
SOX2 SOX9 DAPI
RPC
RGC/HC/AC
SOX2 PAX6 DAPI
HC/AC
PROX1 CALB2 DAPI
BC
CHX10 DAPI
B
RORB
CRX
OTX2
THRB
RXRG
ARR3
MKI67
NR2E3
D0 D30 D45 D60 D75 D90 D105 D120
log2 (FC)
C
ARR3 Ki67 RXRG DAPI
D
ARR3 Ki67 CRX DAPI
hRBOs (Day 60)
hRBOs (Day 90)
E
ARR3 PH3 DAPI
F
ARR3 PCNA DAPI
G
ARR3 SYK DAPI
H
CHOP Ki67 DAPI
Day 60
Day 90
I
ARR3 Ki67 DAPI
NRL Ki67 DAPI
CHX10 Ki67 DAPI
PAX6 SOX2 Ki67 DAPI
PROX1 Ki67 DAPI
Retina
Tumor

Figure S9. Rb in hRBOs originating from maturing cone precursor. (**A**) Immunostaining of rod marker NRL, Müller cell markers SOX2/SOX9, retinal progenitor cell markers SOX2/PAX6, horizontal/amacrine cell markers PROX1, CALB2 and bipolar cell marker CHX10 in hRBOs and hROs at day 105. Scale bar, 50 μm. (**B**) Heatmap showing the average log2-fold difference of genes specific for proliferative cells (*MKI67*), early/immature photoreceptor precursors (*THRB* and *RXRG* for cone; *CRX* and *RORB* for cone or rod), retinal progenitors (*OTX2*); *NR2E3* for rod and maturing cone precursors (ARR3). (**C**) Co-immunostaining of maturing cone precursor marker ARR3 with pan-cone precursor marker RXRG and proliferative marker Ki67 in 90-day-old hRBOs. White arrows indicate $ARR3^{+}/RXRG^{+}/Ki67^{+}$ maturing cone precursors. Yellow arrows indicate $ARR3^{+}/RXRG^{-}/Ki67^{+}$ maturing cone precursors. Asterisks indicate $ARR3^{-}/RXRG^{+}/Ki67^{-}$ cone precursors. Scale bar, 50 μm. (**D**) Co-immunostaining of maturing cone precursor marker ARR3 with early photoreceptor precursor marker CRX and proliferative marker Ki67 in 60- and 90-day-old hRBOs. Magnified views of the boxed regions are shown. White arrows indicate $ARR3^{+}/Ki67^{+}$ maturing cone precursors. Yellow arrows indicate $ARR3^{-}/Ki67^{-}/CRX^{+}$ early photoreceptor precursors. Scale bar, 50 μm. (**E**-**G**) Co-immunostaining of ARR3 with pH3 (**E**) PCNA (**F**) and SYK (**G**) in hRBOs at day 105. Arrows indicate cells co-expressing ARR3 and pH3 (**D**) or PCNA (**E**). Scale bars, 50 μm. (**H**) Co-immunostaining of UPR related protein CHOP with Ki67 in hRBOs at day 60 and 90. Scale bars, 50 μm. (**I**) Co-immunostaining of Ki67 with maturing cone precursor marker ARR3, rod marker NRL, bipolar cell marker CHX10, retinal progenitor cell markers SOX2/PAX6, horizontal cell markers PROX1 in the hRBO-derived intraocular tumors (2 months after subretinal injection). Dashed lines denote the tumor foci. Scale bar, 50 μm.

Figure S10

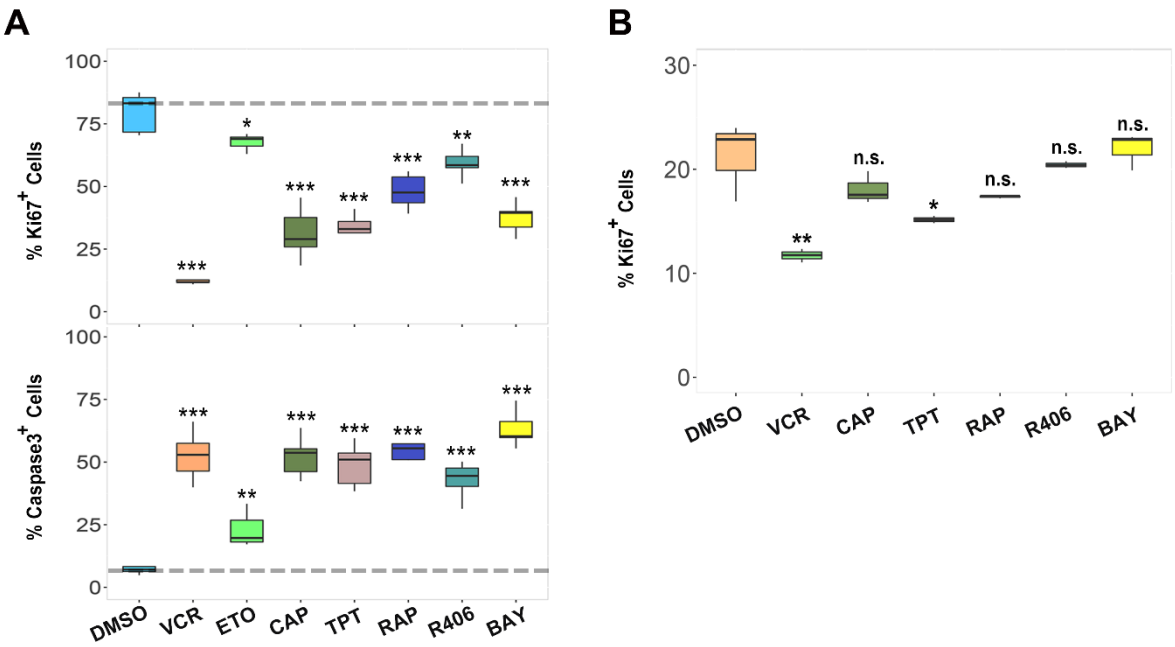

Figure S10. Chemotherapeutic drug responses of hRBOs. (**A**) Quantification of the percentage of Ki67⁺ (Top) and CC3⁺ (Bottom) cells from hRBOs after drug treatments with the indicated drugs as analyzed by immunostaining in Figure 6d. Mean ± SD is shown. n = 5; **P* < 0.05, ***P* < 0.01, ****P* < 0.001. (**B**) Safety testing of six effective drugs in normal hROs. FACS quantification of the percentage of Ki67⁺ cells from hROs after the indicated treatments. Mean ± SD is shown, n=5, ***P* < 0.01, ****P* < 0.001; Statistical analysis was done by one-way ANOVA with Dunnett's test.

Table S1

5′Guide	Score	Sequences (5′-3′)
Guide 1#-C	65	AGGAAAGTTGCTTGAACCCC GGG
Guide 2#	70	ATAGCCAATCAATAGATGAC TGG
Guide 3#	66	CTCTGAGGTTGGAATCACTT TGG
Guide 4#	66	GCGTTAAAAGTCACAGTAGA AGG
Guide 3#-B	60	TTCATTAAGGTTGGGATACA GGG
Guide 5#	80	ACTTGGTTATCAATACCACC AGG
Guide 6#	77	TTCATATACTATTGCCTGCC TGG
Guide 7#	70	GGCAGGCAATAGTATATGAA AGG
Guide 8#-C	53	CTTTTTAATACTGAACAACT TGG
Guide 9#-C	52	CTTTTTTAAATAAACCAGGC AGG
Guide 10#-C	51	GTCAGATGCTTTCTCCCTGG TGG
Guide 11#	50	CCTCTTTGTCATAAACATAA TGG
Guide 12#-C	50	CCATTATGTTTATGACAAAG AGG
Guide 13#-C	49	AAAGTCAGATGCTTTCTCCC TGG
Guide 14#-C	36	GTAGAAACCTAAAATTGGAA TGG

Table S1. sgRNAs targeting *RB1*.

Table S2

Antibodies	Source	Identifier
Anti-Arrestin 3	Novus Biologicals	Cat# NBP1-37003
Anti-ARR3	Sigma-Aldrich	Cat# HPA063129
Anti-RXRγ (A-2)	Santa Cruz Biotechnology	Cat# sc-365252
Anti-Nrl (F-2)	Santa Cruz Biotechnology	Cat# sc-374277
Anti-CHX10	Novus Biologicals	Cat# NBP1-84476
Anti-Sox-2 (E-4)	Santa Cruz Biotechnology	Cat# sc-365823
Anti-SOX9 [EPR14335-78]	Abcam	Cat# ab185966
Anti-Pax-6	Biolegend	Cat# 901301
Anti-Calbindin (D-4)	Santa Cruz Biotechnology	Cat# sc-365360
Anti-Prox 1	Sigma-Aldrich	Cat# AB5475
Anti-Calretinin (H-5)	Santa Cruz Biotechnology	Cat# sc-365956
Anti-Nestin (NES)	BOSTER	Cat# BA1289
Anti-Cleaved Caspase3 (Asp175)	Cell Signaling Technology	Cat# 9664
Anti-Caspase3 (active form)	Millipore	Cat# MAB10753
Anti-Ki67 antibody	Abcam	Cat# ab15580
Anti-Ki-67 Clone B56 (RUO)	BD Biosciences	Cat# 556003
Alexa Fluor 488 Mouse anti-Oct3/4 Clone 40/Oct-3	BD Biosciences	Cat# 560253
Alexa Fluor 647 Mouse anti-Ki-67 Clone B56	BD Biosciences	Cat# 558615
Purified Mouse Anti-Human DEK Clone 2/DEK	BD Biosciences	Cat# 610948
Anti-CDKN2A/p16INK4a	Abcam	Cat# ab108349
Anti-Syk (D3Z1E)	Cell Signaling Technology	Cat# 13198
Anti-Syk (4D10)	Santa Cruz Biotechnology	Cat# sc-1240
Anti-NSE antibody [EPR3377]	Abcam	Cat# ab79757
Anti-Rb antibody [EPR17512]	Abcam	Cat# ab181616
Anti-p53 (DO-1)	Santa Cruz Biotechnology	Cat# sc-126

Anti-Phospho-Histone H3 (Ser10)	Cell Signaling Technology	Cat# 9701
Anti-PCNA (PC10)	Santa Cruz Biotechnology	Cat# sc-56
Anti-CHOP (L63F7)	Cell Signaling Technology	Cat# 2895
Anti-CRX (M02)	Abnove	Cat# ABN-H00001406-M02
Anti-GAPDH	Abcam	Cat# ab181602
DAPI	Thermo Fisher Scientific	Cat# D1306
Donkey anti-Goat IgG (H+L) Secondary Antibody, Alexa Fluor Plus 488	Thermo Fisher Scientific	Cat# A32814
Goat anti-Mouse IgG (H+L) Secondary Antibody, Alexa Fluor Plus 488	Thermo Fisher Scientific	Cat# A32723
Alexa Fluor 594 AffiniPure Donkey Anti-Mouse IgG (H+L)	Jackson ImmunoResearch	Cat# 715-585-151
Donkey anti-Rabbit IgG (H+L) Secondary Antibody, Alexa Fluor 594	Thermo Fisher Scientific	Cat# A-21207
Donkey anti-Goat IgG (H+L) Secondary Antibody, Alexa Fluor 555 conjugate	Thermo Fisher Scientific	Cat# A-21432
IRDye 800CW Goat anti-Mouse IgG Secondary Antibody	LI-COR	Cat# 926-32210
IRDye 800CW Goat anti-Rabbit IgG Secondary Antibody	LI-COR	Cat# 926-32211

Table S2. Antibodies used in this study.

Movie S1. Abnormal proliferation of RB1 mutant hESC-derived hRBOs (days 65-70).

Movie S2. dOCT movie of 105-day-old hRBO.

Movie S3. dOCT movie of 105-day-old hRO.